ARMY RESEARCH LABORATORY

A Computational Framework for Phase-field Modeling

by Jaroslaw Knap and John Clayton

ARL-MR-0760 **January 2011**

NOTICES

Disclaimers

The findings in this report are not to be construed as an official Department of the Army position unless so designated by other authorized documents.

Citation of manufacturer's or trade names does not constitute an official endorsement or approval of the use thereof.

Destroy this report when it is no longer needed. Do not return it to the originator.

ERRATA SHEET

re: ARL-MR-0760, *A Computational Framework for Phase-field Modeling*, January 2011, by Jaroslaw Knap and John Clayton

This is an errata sheet for ARL-MR-0760. Please replace the old version of the report with the new version, and destroy the old version.

Page	Reads	Should Read
2	**Equations 3 and 4 have misplaced/missing characters.**	**Equations 3 and 4 are correct.**
3	**Equation 9 has misplaced/missing characters.**	**Equation 9 is correct.**
4	**Equations 19, 21, 23, 24, and 28 have misplaced/missing characters.**	**Equations 19, 21, 23, 24, and 28 are correct.**
5	**Equation 32 has misplaced/missing characters.**	**Equation 32 is correct.**
6	**Equations 38 and 39 have misplaced/missing characters.**	**Equations 38 and 39 are correct.**

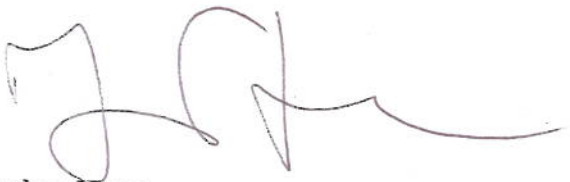

Jaroslaw Knap

U.S. Army Research Laboratory
Computational and Information Sciences Directorate
ATTN: RDRL- CIH-C
Aberdeen Proving Ground, MD 21005

Army Research Laboratory
Aberdeen Proving Ground, MD 21005

ARL-MR-0760 **January 2011**

A Computational Framework for Phase-fielding Modeling

Jaroslaw Knap
Computational and Information Sciences Directorate, ARL

and

John Clayton
Weapons and Materials Research Directorate, ARL

REPORT DOCUMENTATION PAGE	Form Approved OMB No. 0704-0188

1. REPORT DATE *(DD-MM-YYYY)*	2. REPORT TYPE	3. DATES COVERED (From - To)
January 2011	DRI	FY10

4. TITLE AND SUBTITLE
A Computational Framework for Phase-field Modeling

5a. CONTRACT NUMBER

5b. GRANT NUMBER

5c. PROGRAM ELEMENT NUMBER

6. AUTHOR(S)
Jaroslaw Knap and John Clayton

5d. PROJECT NUMBER

5e. TASK NUMBER

5f. WORK UNIT NUMBER

7. PERFORMING ORGANIZATION NAME(S) AND ADDRESS(ES)
U.S. Army Research Laboratory
ATTN: RDRL-CIH-C
Aberdeen Proving Ground, MD 21005

8. PERFORMING ORGANIZATION REPORT NUMBER
ARL-MR-0760

9. SPONSORING/MONITORING AGENCY NAME(S) AND ADDRESS(ES)

10. SPONSOR/MONITOR'S ACRONYM(S)

11. SPONSOR/MONITOR'S REPORT NUMBER(S)

12. DISTRIBUTION/AVAILABILITY STATEMENT
Approved for public release; distribution unlimited.

13. SUPPLEMENTARY NOTES

14. ABSTRACT
As part of the Director's Research Initiative, phase-field theory and simulation software are developed. The theory addresses mechanical twinning in crystalline solids with equilibrium equations obtained via a variational principle in the null temperature limit. Numerical solutions to weak forms of governing equations are obtained via conjugate gradient energy minimization and the finite element (FE) method. Two fundamental problems in materials physics are considered. The first addresses homogeneous nucleation of a twin in a magnesium (Mg) single crystal. Critical shear strains for nucleation obtained numerically using the phase-field approach are in fair agreement with those obtained analytically in the sharp-interface limit. The second addresses twin nucleation in calcite ($CaCO_3$) single crystals subjected to indentation loading. Long, thin, asymmetric twins with sharp cusp-like tips are observed in the numerical simulations and are in qualitative agreement with experiments. All results obtained are predictive; the model does not require calibration or fitting of material parameters.

15. SUBJECT TERMS
Computational mechanics, phase-field, scientific computing

16. SECURITY CLASSIFICATION OF:			17. LIMITATION OF ABSTRACT	18. NUMBER OF PAGES	19a. NAME OF RESPONSIBLE PERSON
a. REPORT	b. ABSTRACT	c. THIS PAGE			Jaroslaw Knap
Unclassified	Unclassified	Unclassified	UU	28	19b. TELEPHONE NUMBER (*Include area code*) (410) 278-0520

Contents

List of Figures

List of Tables

Acknowledgment

Dr. Michael Greenfield of the U.S. Army Research Laboratory (ARL) Weapons and Materials Research Directorate (WMRD) is acknowledged for suggesting study of the problem of elastic twinning in transparent calcite.

INTENTIONALLY LEFT BLANK.

1. Objective

The objective of this research is to develop a computational capability for large-scale parallel simulations of microstructure evolution in crystalline solids. The task-oriented goals are to (1) design a flexible computational finite element (FE) framework for phase-field modeling; (2) implement this framework on the large-scale computing platforms maintained by the High Performance Computing Modernization Office (HPCMO); and (3) perform verification and validation (V&V) simulations, focusing on the problem of mechanical twinning in lightweight materials of interest to the U.S. Army Research Laboratory (ARL). Simulations are intended to provide new insight into behavior of lightweight metals and ceramics concurrently under development in the Weapons and Materials Research Directorate (WMRD) for vehicular armor and personnel protection applications.

2. Approach

The technical approach consists of the following two steps: (1) development of a new phase-field theory for deformation twinning in crystalline solids and (2) implementation and testing of the theory in FE software. Each of these steps is summarized in a separate section in what follows.

2.1 Phase-field Theory

A complete description of the phase-field theory developed by the authors will be available in a forthcoming article (*1*). The theory is summarized below, following a brief introduction. Standard notational conventions of continuum mechanics are used.

Phase-field models have been successfully applied towards a variety of problems in materials science, chemistry, and physics. At each point in the problem domain, one or more phase-field variables describe the state of the substance. The term "phase" here denotes a certain crystal structure or lattice configuration. In regions of uniform phase, order parameters acquire discrete values of zero or one. In interfacial regions, order parameters enable interpolation between pure phases. In addition to depending on usual mechanical and thermal state variables (e.g., strain and temperature), the free energy density of a substance generally depends on local value(s) of order parameter(s) and spatial gradients of order parameter(s). Surface energies of phase boundaries can be directly associated with order parameter gradients in interfacial regions.

Cahn and Hilliard (*2*) and Allen and Cahn (*3*) studied thermodynamics and kinetics of heterogeneous material systems in the context of phase-field models. In traditional phase-field modeling, it is typically assumed that a material system will tend to evolve towards a state of minimum free energy, subject to boundary constraints imposed on the system. Concepts for

modeling multiphase systems were advanced by Steinbach et al. (*4*) and Steinbach and Apel (*5*). Fried and Gurtin (*6*) and Gurtin (*7*) developed order parameter theories incorporating configurational forces in the context of geometrically nonlinear continuum mechanics and thermodynamics. Review articles describe numerical techniques and applications (*8, 9*).

Mathematically, a scalar order parameter field is denoted by $\eta(\mathbf{X},t)$, with $\mathbf{X}$ material coordinates and t time. The two distinct phases represented are the original crystal (i.e., the parent) and the twin, with interfaces between phases representing twin boundaries. In terms of the order parameter,

$$\eta = 0 \ \forall \mathbf{X} \in \text{parent};\ \eta = 1 \ \forall \mathbf{X} \in \text{twin};\ 0 < \eta < 1 \ \forall \mathbf{X} \in \text{interfacial regions}. \tag{1}$$

Let $\mathbf{x} = \mathbf{x}(\mathbf{X},t) = \mathbf{X} + \mathbf{u}(\mathbf{X},t)$ denote spatial coordinates of a material particle, with $\mathbf{u}$ the displacement. The deformation gradient $\mathbf{F}$ is

$$\mathbf{F} = \nabla \mathbf{x},\ F_{aA} = \nabla_A x_a, \tag{2}$$

with $\nabla_A = \partial / \partial X_A$ the material gradient. Deformation gradient (equation 2) is further decomposed as

$$\mathbf{F} = \mathbf{F}^{\mathbf{E}}\mathbf{F}^{\boldsymbol{\eta}}, \tag{3}$$

where

$$\mathbf{F}^{\mathbf{E}}(\mathbf{X},t) = \mathbf{F}\mathbf{F}^{\boldsymbol{\eta}-1} \coloneqq \text{ elastic deformation};\ \mathbf{F}^{\boldsymbol{\eta}}[\eta(\mathbf{X},t)] \coloneqq \text{ "stress-free" twinning shear}. \tag{4}$$

Specifically, the twinning shear is interpolated in interfacial regions as follows:

$$\mathbf{F}^{\boldsymbol{\eta}} = \mathbf{1} + [\varphi(\eta)]\gamma_0 \mathbf{s} \otimes \mathbf{m}, \tag{5}$$

where φ is an interpolation function obeying $0 \le \varphi \le 1,\ \varphi(0) = 0,\ \varphi(1) = 1,\ \varphi$ is monotone. A representative function also satisfying $(\partial\varphi/\partial\eta)\big|_{\eta=0} = (\partial\varphi/\partial\eta)\big|_{\eta=1} = 0$ used later is (*10*)

$$\varphi = \alpha\eta^2 + 2(2-\alpha)\eta^3 + (\alpha-3)\eta^4, \tag{6}$$

where α is a scalar constant within the limits $0 < \alpha < 6$. The total free energy functional for a body of reference volume Ω is written as

$$\Psi = \int_{\Omega} W(\mathbf{F},\eta)\, d\Omega + \int_{\Omega} f(\eta, \nabla\eta)\, d\Omega, \tag{7}$$

where W is the elastic strain energy density (generally non-zero in parent, twin, and interfacial regions), and where f accounts for interfacial energy in twin boundary regions. Strain energy per unit reference volume is of the functional form

$$W = W[\mathbf{E}^{\mathbf{E}}(\mathbf{F},\eta),\eta],\ \mathbf{E}^{\mathbf{E}} = (1/2)(\mathbf{C}^{\mathbf{E}} - \mathbf{1}) = (1/2)(\mathbf{F}^{\mathbf{E}T}\mathbf{F}^{\mathbf{E}} - \mathbf{1}), \tag{8}$$

with $\mathbf{C}^{\mathbf{E}}$ the elastic deformation tensor, $\mathbf{E}^{\mathbf{E}}$ the elastic strain tensor, and a superposed *T* denoting the transpose. For any value of η, strain energy density vanishes at null elastic strain:

$$W(0,\bullet) = 0\,. \tag{9}$$

A quadratic form for the strain energy density is assumed. Higher-order elastic coefficients can be incorporated by extension (*11*). Dependence of $W(\mathbf{E}^{\mathbf{E}},\eta)$ on η manifests explicitly only via anisotropic elastic coefficients. Strain energy density and second-order moduli are written

$$W = (1/2)\mathbf{E}^{\mathbf{E}} : \mathbf{C}(\eta) : \mathbf{E}^{\mathbf{E}},\ \mathbf{C}(\eta) = \partial^2 W/(\partial\mathbf{E}^{\mathbf{E}}\partial\mathbf{E}^{\mathbf{E}})\big|_{\mathbf{E}^{\mathbf{E}}=0}\,. \tag{10}$$

As usual, indices $C_{ABCD} = C_{BADC} = C_{CDAB}$ and the Laue group of the crystal dictate any other symmetries of $\mathbf{C}(0)$ in the crystallographic frame of reference. For a compound twin in a centrosymmetric structure, reorientation matrix $\mathbf{Q}$ associated with twinning is (*12*)

$$\mathbf{Q} = 2\mathbf{m}\otimes\mathbf{m} - \mathbf{1}\,. \tag{11}$$

Elastic coefficients of the fully twinned crystal are related to those of the parent by

$$C_{ABCD}(1) = Q_{AE}Q_{BF}Q_{CG}Q_{DH}C_{EFGH}(0)\,. \tag{12}$$

Elastic coefficients in interfacial regions are interpolated the same way as the twinning shear:

$$\mathbf{C}(\eta) = \mathbf{C}(0) + [\mathbf{C}(1) - \mathbf{C}(0)]\varphi\,, \tag{13}$$

where $\varphi(\eta)$ obeys equation 6. In the isotropic elastic approximation, letting λ denote Lamé's constant and μ the shear modulus, the elasticity tensor

$$C_{ABCD} = \lambda\delta_{AB}\delta_{CD} + \mu(\delta_{AC}\delta_{BD} + \delta_{AD}\delta_{BC})\,, \tag{14}$$

so that $\mathbf{C}(0) = \mathbf{C}(1)$ and $W(\mathbf{E}^{\mathbf{E}},\eta) \to W(\mathbf{E}^{\mathbf{E}})$ does not explicitly depend on η. The local interfacial energy per unit reference volume follows the Cahn-Hilliard formalism (*2*):

$$f(\eta,\nabla\eta) = f_0(\eta) + \boldsymbol{\kappa} : (\nabla\eta\otimes\nabla\eta)\,, \tag{15}$$

with $\boldsymbol{\kappa}$ a symmetric second-order tensor, here assumed constant. When interfacial energy is isotropic, $\boldsymbol{\kappa} = \kappa\mathbf{1}$ and

$$f(\eta,\nabla\eta) = f_0(\eta) + \kappa\,|\nabla\eta|^2\,. \tag{16}$$

Prescribed for f_0 is a standard "double-well" potential (*6, 8*):

$$f_0 = A\eta^2(1-\eta)^2\,, \tag{17}$$

with *A* a non-negative constant. As shown in reference 1, in the isotropic approximation *A* and κ are related to equilibrium energy per unit area Γ and thickness *l* of an unstressed interface via

$$\kappa = 3\Gamma l/4,\ A = 12\Gamma/l. \tag{18}$$

The total free energy functional Ψ of equation 7 becomes, using equations 10 and 15:

$$\Psi = (1/2)\int_{\Omega} \mathbf{E}^{\mathbf{E}} : \mathbf{C}(\eta) : \mathbf{E}^{\mathbf{E}} d\Omega + \int_{\Omega} [A\eta^2(1-\eta)^2 + \boldsymbol{\kappa} : (\nabla\eta \otimes \nabla\eta)] d\Omega. \tag{19}$$

For isotropic elastic and interfacial energies,

$$\Psi = \int_{\Omega} [(\lambda/2)(\mathrm{tr}\mathbf{E}^{\mathbf{E}})^2 + \mu \mathbf{E}^{\mathbf{E}} : \mathbf{E}^{\mathbf{E}}] d\Omega + \int_{\Omega} [A\eta^2(1-\eta)^2 + \kappa |\nabla\eta|^2] d\Omega. \tag{20}$$

The following variational equation is posited that will suggest, upon application of Hamilton's principle, local or strong forms of static equilibrium equations and boundary conditions:

$$\delta\Psi - \int_{\partial\Omega} \mathbf{t} \bullet \delta\mathbf{x} dS - \int_{\partial\Omega} h\delta\eta dS = 0, \tag{21}$$

where **t** is a mechanical traction vector per unit reference area, dS is a surface element of Ω, and h is a scalar conjugate force to variations of the order parameter. Taking the first variation of the interfacial energy and applying the divergence theorem,

$$\delta\int_{\Omega} f d\Omega = \int_{\Omega} (\partial f_0/\partial\eta)\delta\eta dV - \int_{\Omega} 2\boldsymbol{\kappa} : [\nabla(\nabla\eta)]\delta\eta d\Omega + \int_{\partial\Omega} 2\boldsymbol{\kappa} : [(\nabla\eta) \otimes \mathbf{n}]\delta\eta dS, \tag{22}$$

with **n** the unit outward normal to $\partial\Omega$. Taking the first variation of the strain energy with **F** and η independent,

$$\delta\int_{\Omega} W d\Omega = \int_{\Omega} (\partial W/\partial\eta)\delta\eta d\Omega - \int_{\Omega} [\nabla \bullet (\partial W/\partial\mathbf{F})] \bullet \delta\mathbf{x} d\Omega + \int_{\partial\Omega} [\mathbf{n} \bullet (\partial W/\partial\mathbf{F})] \bullet \delta\mathbf{x} dS. \tag{23}$$

It follows that within Ω, Euler-Lagrange equations are

$$\nabla \bullet (\partial W/\partial\mathbf{F})\big|_{\eta} = \nabla \bullet \mathbf{P} = 0,\ \nabla_A (\partial W/\partial\nabla_A x_a)\big|_{\eta} = \nabla_A P_{aA} = 0; \tag{24}$$

$$\partial f_0/\partial\eta - 2\boldsymbol{\kappa} : [\nabla(\nabla\eta)] + (\partial W/\partial\eta)\big|_{\mathbf{F}} = 0,\ \partial f_0/\partial\eta - 2\kappa_{AB}\nabla_A\nabla_B\eta + (\partial W/\partial\eta)\big|_{\mathbf{F}} = 0; \tag{25}$$

where **P** is the first Piola-Kirchhoff stress tensor. Corresponding boundary conditions are

$$\mathbf{t} = \mathbf{P}\mathbf{n},\ t_a = P_{aA}n_A; \tag{26}$$

$$h = 2\boldsymbol{\kappa} : (\nabla\eta \otimes \mathbf{n}),\ h = 2\kappa_{AB}n_B\nabla_A\eta. \tag{27}$$

The first Piola-Kirchhoff stress also obeys

$$\mathbf{P} = (\partial W/\partial\mathbf{F})\big|_{\eta} = (\partial W/\partial\mathbf{E}^{\mathbf{E}}) : (\partial\mathbf{E}^{\mathbf{E}}/\partial\mathbf{F}^{\mathbf{E}}) : (\partial\mathbf{F}^{\mathbf{E}}/\partial\mathbf{F})\big|_{\eta} = \mathbf{F}^{\mathbf{E}}\boldsymbol{\Sigma}\mathbf{F}^{\boldsymbol{\eta}-T}. \tag{28}$$

The elastic second Piola-Kirchhoff stress is

$$\boldsymbol{\Sigma} = \partial W / \partial \mathbf{E}^{\mathbf{E}} = \mathbf{C} : \mathbf{E}^{\mathbf{E}}. \tag{29}$$

The partial derivative of $W[\mathbf{E}^{\mathbf{E}}(\mathbf{F},\eta),\eta]$ with $\mathbf{F}$ fixed is computed as

$$(\partial W / \partial \eta)\big|_{\mathbf{F}} = (\partial W / \partial \eta)\big|_{\mathbf{E}^{\mathbf{E}}} + (\partial W / \partial \mathbf{E}^{\mathbf{E}})\big|_{\eta} : (\partial \mathbf{E}^{\mathbf{E}} / \partial \eta)\big|_{\mathbf{F}}. \tag{30}$$

Furthermore,

$$(\partial W / \partial \eta)\big|_{\mathbf{E}^{\mathbf{E}}} = (1/2)\mathbf{E}^{\mathbf{E}} : (\partial \mathbf{C} / \partial \eta) : \mathbf{E}^{\mathbf{E}} = (1/2)(\partial \varphi / \partial \eta)\mathbf{E}^{\mathbf{E}} : [\mathbf{C}(1) - \mathbf{C}(0)] : \mathbf{E}^{\mathbf{E}}, \tag{31}$$

$$(\partial W / \partial \mathbf{E}^{\mathbf{E}})\big|_{\eta} : (\partial \mathbf{E}^{\mathbf{E}} / \partial \eta)\big|_{\mathbf{F}} = -\{\boldsymbol{\Sigma} : [\mathbf{C}^{\mathbf{E}}(\mathbf{s} \otimes \mathbf{m})\mathbf{F}^{\boldsymbol{\eta}-1}]\}\gamma_0(\partial \varphi / \partial \eta) = -\tau \gamma_0 (\partial \varphi / \partial \eta). \tag{32}$$

It can be verified that τ is a kind of resolved shear stress on the habit plane in the direction of twinning shear. Phase equilibrium condition (equation 25) can be rewritten

$$\partial f_0 / \partial \eta - 2\boldsymbol{\kappa} : [\nabla(\nabla \eta)] = \{(1/2)\mathbf{E}^{\mathbf{E}} : [\mathbf{C}(0) - \mathbf{C}(1)] : \mathbf{E}^{\mathbf{E}} + \tau \gamma_0\}(\partial \varphi / \partial \eta). \tag{33}$$

In the isotropic approximation, choosing φ from equation 6 and f_0 from equation 17, equation 33 becomes

$$\tau[\alpha \eta + 3(2-\alpha)\eta^2 + 2(\alpha - 3)\eta^3] = (1/\gamma_0)[A\eta(1 - 3\eta + 2\eta^2) - \kappa \nabla^2 \eta]. \tag{34}$$

Both sides of equation 34 vanish identically in regions of uniform phase where $\eta = 0$ or $\eta = 1$.

The preceding derivations focus on the geometrically nonlinear theory, with only a single twin system (i.e., a single order parameter). Geometric linearization of the theory, extension of the theory to account for multiple twin systems (i.e., multiple order parameters), and existence of solutions to the energy minimization problem corresponding to equation 21 are discussed in reference 1.

2.2 Finite Element Formulation

The FE method is used to seek solutions for equilibrium or local minimum energy states of a body subjected to boundary conditions. At each reference point **X**, primary solution variables are displacement **u** and order parameter η. If these variables and requisite material properties are known, then all elastic field variables and interfacial quantities can be computed via mathematical operations given in section 2.1.

The body of reference volume Ω is discretized into a number of standard FEs with shape functions $N_i(\mathbf{X})$. Let $\mathbf{u}_i(t)$ and $\eta_i(t)$ denote instantaneous values of displacement and order parameter, respectively, at node *i*. Displacement and order parameter fields are represented in a FE context as

$$\mathbf{u}(\mathbf{X},t) = \mathbf{u}_i(t) N_i(\mathbf{X}),\ \eta(\mathbf{X},t) = \eta_i(t) N_i(\mathbf{X}), \tag{35}$$

where summation proceeds over all nodes *i*; however, only those nodes supporting the element(s) containing or bounding point **X** have $N_i(\mathbf{X}) \neq 0$. Material gradients of equation 35 follow as

$$\mathbf{F} = \mathbf{1} + \nabla \mathbf{u} = \mathbf{1} + \mathbf{u}_i \otimes \nabla N_i, \ \nabla \eta = \eta_i \nabla N_i. \tag{36}$$

The FE method is used to seek solutions of global or weak forms of the equilibrium conditions. Strong (local) forms are not needed by the numerical algorithms. Addressed in what follows are the following kinds of boundary conditions:

$$\left.\begin{array}{l} \partial\Omega = \partial\Omega_M \cap \partial\Omega_P; \\ \partial\Omega_M = \partial\Omega_{M,D} \cup \partial\Omega_{M,N}, \varnothing = \partial\Omega_{M,D} \cap \partial\Omega_{M,N}; \\ \mathbf{u}(\mathbf{X},t) \text{ prescribed on } \partial\Omega_{M,D}, \ \mathbf{t}(\mathbf{X},t) = 0 \text{ on } \partial\Omega_{M,N}; \end{array}\right\} \text{mechanical conditions}$$
$$\left.\begin{array}{l} \partial\Omega_P = \partial\Omega_{P,D} \cup \partial\Omega_{P,N}, \varnothing = \partial\Omega_{P,D} \cap \partial\Omega_{P,N}; \\ \eta(\mathbf{X},t) \text{ prescribed on } \partial\Omega_{P,D}, \ h(\mathbf{X},t) = 0 \text{ on } \partial\Omega_{P,N}. \end{array}\right\} \text{phase field conditions} \tag{37}$$

Dirichlet conditions for displacement and the order parameter are applied on $\partial\Omega_{M,D}$ and $\partial\Omega_{P,D}$, respectively. Neumann conditions corresponding to free surfaces are applied on $\partial\Omega_{M,N}$ and $\partial\Omega_{P,N}$, respectively. The present treatment can be extended to address arbitrary Neumann conditions if terms accounting for external work are incorporated in the total energy functional whose stationary points are sought.

The free energy functional is equation 19 in the general anisotropic case. Nodal equilibrium conditions are obtained by substituting equations 35 and 36 into equation 19 and differentiating with respect to nodal degrees of freedom:

$$0 = \partial \Psi / \partial \mathbf{u}_i = \int_\Omega \mathbf{P} \nabla N_i d\Omega = \int_\Omega [\mathbf{F}^{\mathbf{E}}(\mathbf{C} : \mathbf{E}^{\mathbf{E}})\mathbf{F}^{\boldsymbol{\eta}-T}] \nabla N_i d\Omega, \tag{38}$$

$$\begin{aligned} 0 = \partial \Psi / \partial \eta_i = & \int_\Omega \left\{ 2A\eta(1 - 3\eta + 2\eta^2) \right\} N_i d\Omega + \int_\Omega \left\{ 2\boldsymbol{\kappa} \nabla \eta \right\} \bullet \nabla N_i d\Omega \\ & + \int_\Omega \left\{ (1/2)\mathbf{E}^{\mathbf{E}} : [\mathbf{C}(1) - \mathbf{C}(0)] : \mathbf{E}^{\mathbf{E}} - \tau\gamma_0 \right\} (\partial\varphi / \partial\eta) N_i d\Omega. \end{aligned} \tag{39}$$

A conjugate gradient algorithm is used to seek minimum energy states corresponding to equations 38 and 39, following prescription of initial conditions.

2.3 Phase-field Software Framework

The above FE numerical formulation is implemented into a standalone software framework. In contrast with more commonly employed approaches relying on a single executable to handle all variability in problems and data, our computational framework enables users to rapidly develop applications tailored to their particular needs. This flexibility is achieved through modern software development design and practices. The core computational kernels (e.g., FE methodology, quadrature integration rules, phase-field energy densities, and minimization

solvers) are implemented in ANSI C++, which affords great code portability, modularity, and code reuse. In contrast, high-level user-interfaces are accessible both from C++ and Python for rapid application development. The modular structure of the framework greatly simplifies extension efforts, for example, adding new models of material or interface behavior. Moreover, such structure allows for a wide spread use of generic programming concepts that enable separation of algorithms from the data on which they operate. By way of example, we implemented a family of generic nonlinear minimization solvers (Jacobi-preconditioned conjugate-gradient and Newton-Raphson) that can be employed to solve problems derived from the FE method, as well as those characterized by an explicit function. Input and output are handled exclusively via ARL's Extensible Data Model and Format (XDMF) (*25*). Input consists of a FE domain discretization (mesh) along with model parameters contained in an XDMF file. Owing to the fact that XDMF contains filters from popular computer-aided design (CAD) mesh formats, external off-the-shelf meshing tools can be employed. An output file contains a snapshot of the entire internal state of a phase-field application and thus can be used to resume its execution. In addition, the output file may be used for visualization purposes as many visualization packages are able to directly read XMDF files.

The phase-field software framework can take advantage of large-scale distributed memory high-performance computers (HPCs) by recourse to the Message Passing Interface (MPI) (*26*). Our implementation relies on conventional non-overlapping domain decomposition methodology (*27*) in which a FE mesh is distributed among processors and compatibility conditions are enforced across sub-domain boundaries. Mesh decomposition is carried out via a set of XDMF tools that perform mesh partitioning as well as establish mappings between shared mesh vertices on all sub-domain boundaries. The main advantage of the non-overlapping domain decomposition methodology is it relative simplicity and limited scope of modifications to serial implementations while still offering remarkable performance and scalability on modern HPC systems.

3. Results

3.1 Twin Nucleation in Magnesium

Homogeneous twin nucleation refers to creation of a twin embryo within an otherwise perfect single crystal (*12*). Analytical models based on free energy variations in the context of phase transformations have been applied to describe twin nucleation (*12, 13*). Such approaches consider nucleation of a twin embryo of idealized geometry—an elliptical cylinder in two dimensions or an ellipsoid in three dimensions—embedded in an infinite medium, with a perfectly bonded sharp interface separating inclusion from surrounding medium (i.e., the matrix). The solution technique involves simultaneous solution of two equilibrium equations associated with stationary points of the Gibbs free energy change associated with twinning. These two

equations yield the critical size and aspect ratio of the inclusion, as outlined in references 1 and 13. Apparently, exact solutions are available only for the approximations of linear elasticity, isotropic surface energy associated with the twin boundary, and traction boundary conditions at infinity. The solution provides the critical size and shape of an inclusion for a given set of material properties—elastic constants, twin boundary surface energy, and twinning transformation shear—and far-field applied stress. At the critical aspect ratio, the critical size corresponds to unstable equilibrium, i.e., a saddle point on the free energy surface. At a given far-field applied stress, a twin nucleus smaller than the critical size will tend to shrink and disappear, while one larger than the critical size will tend to grow in an unstable manner. The larger the applied stress component resolved on the habit plane in the twinning direction, the smaller the critical size, meaning that nucleation of a twin of fixed size becomes more energetically favorable as the resolved shear stress increases.

The phase-field approach is used in the present work to model the problem of homogeneous twin nucleation. Numerical results obtained from the phase-field model, under assumptions of geometric linearity and plane strain boundary conditions, are compared with the analytical solution (*13*). This exercise provides validation for the phase-field model and numerical methods advanced here. Additional numerical simulations consider effects of anisotropic twin boundary surface energy, variable equilibrium thickness of the twin boundary region, various habit plane directions (i.e., lattice orientations), and various boundary conditions (Dirichlet vs. Neumann, shear vs. tension, and domain shapes). These additional factors cannot all be addressed via known analytical elasticity solution techniques.

Pure magnesium (Mg) single crystals are studied. Mg, a metallic crystalline solid at standard temperature and pressure, is of particular interest for lightweight vehicular protection applications because of its low mass density. Properties are listed in table 1 with supporting references. Mg exhibits a hexagonal crystal structure and is centrosymmetric, with c/a ratio 1.6235. The twinning system of consideration is the primary one: $<10\bar{1}1>\{\bar{1}012\}$ with twinning shear $\gamma_0 = (3 - c^2/a^2)/(3^{1/2} c/a) = 0.1295$. Voigt averages are used for isotropic elastic constants. Mg single crystals are nearly isotropic elastically [$C_{11} \approx C_{33}$, $C_{12} \approx C_{13}$, and $C_{44} \approx (C_{11} - C_{12})/2$], so this isotropic elastic approximation is reasonable.

Table 1. Properties for pure Mg single crystals.

Parameter	Value	Definition	Reference
γ_0	0.1295	Shear for $<10\bar{1}1>\{\bar{1}012\}$ twin	12
λ	24.0 GPa	Lamé constant (Voigt average, 0 K)	14
μ	19.4 GPa	Shear modulus (Voigt average, 0 K)	14
Γ	117 mJ/m^2	Twin boundary energy (0 K)	15
l	1.0 nm	Equilibrium boundary thickness	16

Sought are critical applied strains for twin nucleation for the simulation cases listed in table 2, which encompass various boundary conditions, material properties, and lattice orientations. Here, *L/H* denotes the aspect ratio of the simulation domain, where *H* is fixed at 50 nm. Critical strains are obtained in practice by seeding the domain with an inclusion of initial radius $a_0 = 3$ nm (which is on the order of the minimum stable size observed from first principles calculations [*15*]), as shown in figure 1, and then applying the boundary deformation in small increments of magnitude 0.001. For each increment, system degrees of freedom relax in conjunction with energy minimization, performed numerically via the conjugate gradient technique. The minimum applied strain for which decay in size of the twin/inclusion does not occur is deemed the critical strain γ_C. The corresponding average shear stress is τ_C.

Table 2. Phase-field simulation parameters, predicted critical strain for twin nucleation γ_C, and average equilibrium shear stress τ_C after twin has fully grown.

Case	θ rad	l nm	κ_{11}/κ_{22}	L / H	Boundary	Loading	γ_C	τ_C/μ
1	0	1	1	1	Dirichlet	shear	0.050	0.020
2	0	1	1	1	Neummann	shear	0.050	0.000
3	0	1	1	1.5	Dirichlet	shear	0.049	0.012
4	0	1	4[a]	1	Dirichlet	shear	0.046	0.023
5	0	0.1	1	1	Dirichlet	shear	0.049	0.044
6	π/6	1	1	1	Dirichlet	shear	0.050	0.042
7	π/4	1	1	1	Neummann	tension	0.045	0.005

[a]Anisotropic surface energy: $\kappa_{11}/2 = 2\kappa_{22} = \kappa$.

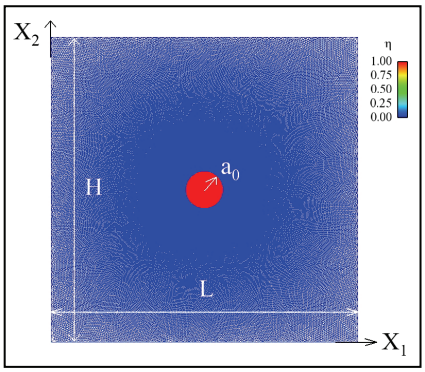

Figure 1. FE mesh and initial conditions of an undeformed shape.

Figure 2 shows equilibrium order parameter contours for each simulation at the applied critical strain. Figure 3 shows corresponding shear stresses. For cases 1–6, the local shear stress shown is σ_{12}; for case 7, the stress shown is that acting on a 45° plane, $(\sigma_{22} - \sigma_{11})/2$. Results are mesh-insensitive except for those of case 5, wherein growth of the twin is confined to the center of the domain where the mesh is refined enough to resolve gradients of the order parameter at the interface. Predictions of critical nucleation strain from the phase-field simulations are compared with predictions of other models in table 3.

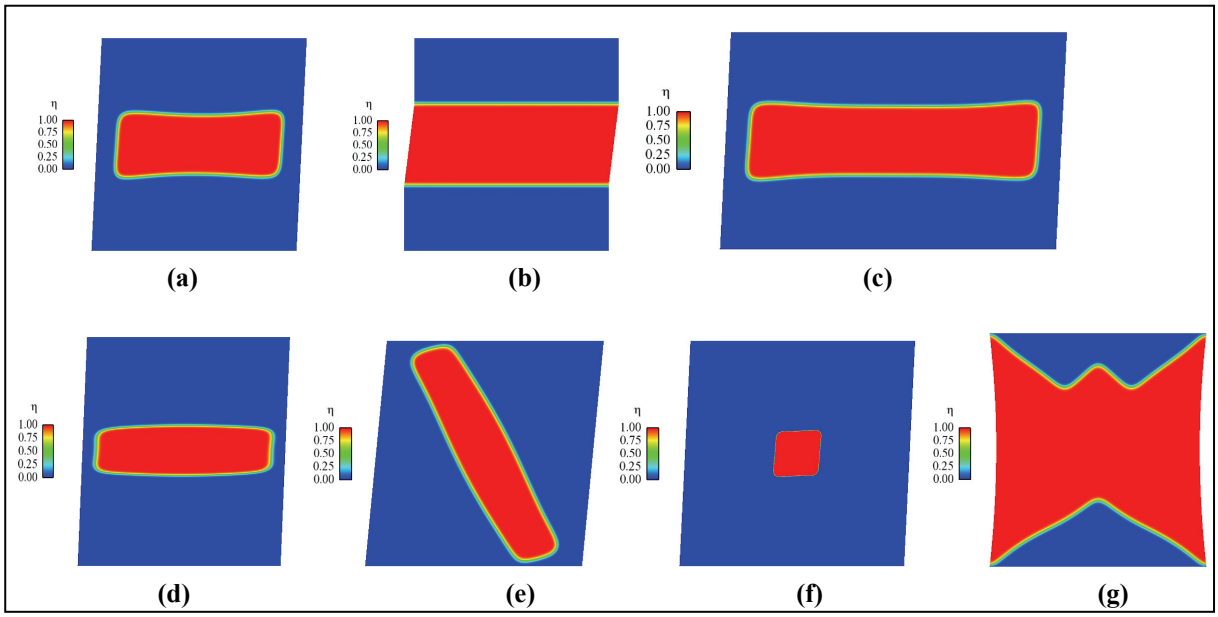

Figure 2. Equilibrium order parameter field (fully formed twin) at critical strain for simulations listed in table 2: (a) case 1, (b) case 2, (c) case 3, (d) case 4, (e) case 5, (f) case 6, and (g) case 7.

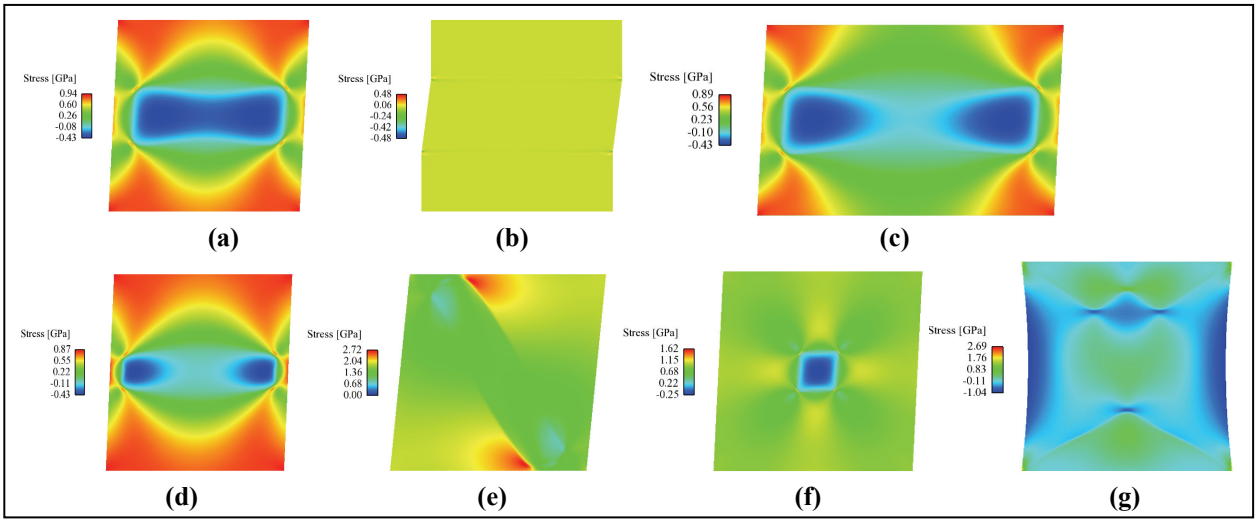

Figure 3. Equilibrium effective shear stress field (fully formed twin) at critical strain for simulations listed in table 2: (a) case 1, (b) case 2, (c) case 3, (d) case 4, (e) case 5, (f) case 6, and (g) case 7.

Table 3. Critical strain for twin nucleation or growth: comparison with other models.

Model	Reference	Remarks	γ_C
Phase-field	This work	Cases 1–7, Table 2	0.045-0.050
Elastic inclusion	13	Analytical solution, infinite medium	0.038
Theoretical strength	17	$\gamma_C = \gamma_0/(2\pi)$	0.021
Atomic calculation	18	Glide of $1/17[10\bar{1}1](\bar{1}012)$ partial	0.004

3.2 Twin Nucleation in Calcite

Considered next is the problem of twin nucleation in calcite ($CaCO_3$). $CaCO_3$ is of interest for a number of reasons. Experiments in the 1930s through the 1960s, conducted primarily in the Soviet Union (*19, 20*), demonstrated the phenomenon of elastic twinning in $CaCO_3$ single crystals subjected to concentrated surface loading, e.g., indentation. Elastic twins partially or fully disappear upon load removal. This phenomenon is realistically modeled by the present phase field approach that considers twinning in the non-dissipative and null temperature (0 K) limit. $CaCO_3$ is an ideal material for the study of twinning because it is transparent (hence twins are easily observed) and exhibits little plasticity (i.e., uncorrelated slip of dislocations) or fracture, relative to twinning, at low temperatures. Requisite properties of $CaCO_3$ are listed in table 4 with supporting references.

Table 4. Properties for pure $CaCO_3$ single crystals.

Parameter	Value	Definition	Reference
γ_0	0.694	Shear for e^+ twin	21
λ	61.7 GPa	Lamé constant (Voigt average, 0 K)	22
μ	40.2 GPa	Shear modulus (Voigt average, 0 K)	22
Γ	183 mJ/m^2	Twin boundary energy (0 K)	23
l	1.0 nm	Equilibrium boundary thickness	23

The problem of study is illustrated schematically in figure 4(a). A single crystal oriented for twinning is subjected to concentrated surface loading via a wedge-shaped indenter. The indenter is assumed to adhere rigidly to the crystal surface. The crystallography and coordinate system are discussed in more detail in reference 11.

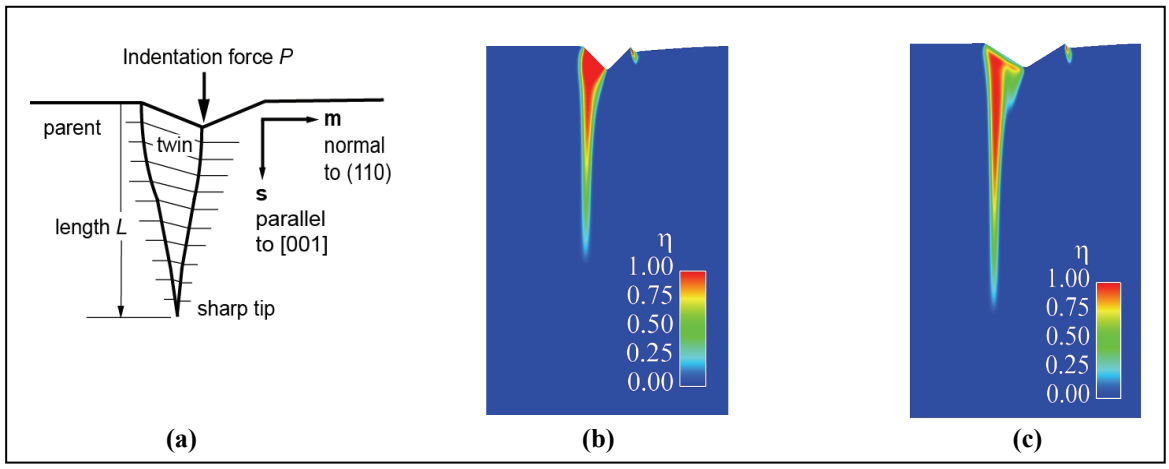

Figure 4. Indentation of $CaCO_3$ single crystal oriented for twinning: (a) sketch of boundary value problem (*19*) and predicted order parameter field from phase-field simulations: (b) 90° wedge and (c) 120° wedge.

Contours of the order parameter field predicted from phase-field simulations are shown in figures 4(b) and 4(c). The indentation depth is 4.75 nm. Notice that in each case the major twin forms asymmetrically under only one side of the indenter because the shear deformation on the

opposite side is directed in the anti-twinning sense. The twin shapes are long and thin, with sharp tips, as observed in experiments (*19, 20*). It is found that the threshold for twin nucleation is highly sensitive to the presence of initial defects in $CaCO_3$, and that the length L of the twin increases monotonically with increasing load P. Both such trends in results have also been observed experimentally (*19, 20, 24*). Also noteworthy are the small secondary twins that appear spontaneously on the right side of the indenter, at the free surface.

Results shown in figures 4(b) and 4(c) are obtained using the phase field theory under the approximation of linear isotropic elasticity. A more complete study of twinning in $CaCO_3$ single crystals using the phase field approach will appear in a forthcoming publication (*11*), which will also incorporate nonlinear and anisotropic elasticity. $CaCO_3$ is of Army interest because it is a lightweight nonmetallic mineral with ductility (i.e., a kind of "soft ceramic") whose study may provide qualitative insight into inelastic phenomena that arise in other transparent ceramics (used for armor applications) that undergo twinning such as alumina (Al_2O_3) and aluminum oxynitride (AlON). $CaCO_3$ belongs to the same crystallographic space group as α-alumina (i.e., sapphire); both belong to centrosymmetric point groups with trigonal symmetry.

3.3 Parallel Performance

We investigated parallel performance of the phase-field software framework for the problem of twin nucleation in magnesium (see figure 1). Our measurements were performed on MJM HPC system located at ARL's Department of Defense (DoD) Supercomputing Resource Center.

The first performance test was focused on the measurement of parallel speedup. Parallel speedup, S_p is commonly defined as

$$S_p = \frac{T_1}{T_p}, \tag{40}$$

where: T_1, T_p denote the execution time of the sequential and parallel algorithm on p processors, respectively. We measured S_p for two discretizations of the computational domain containing 257,094 and 502,780 linear triangular elements and the number of processors in the 1 to 2048 range. The speedup as a function of the numbers of processors is plotted in figure 5(a) along with the ideal speedup ($S_p = p$). Close to ideal parallel speedup may be observed in the 1 to 512 processor range. Outside this range (for processor counts larger than 512) the speedup is markedly reduced. This behavior is expected as the average number of elements per processor for 1024 processors is reduced to merely 251 and 490, respectively. Under such circumstances the computational expense becomes significantly influenced by the cost of inter-processor communication.

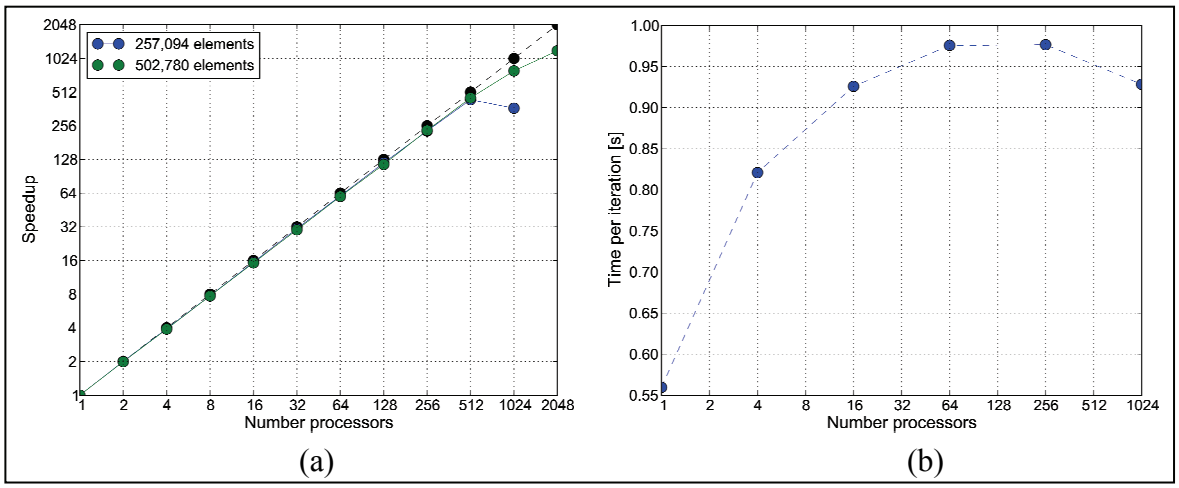

Figure 5. (a) Measured values of parallel speedup vs. number of processors and (b) execution time per one conjugate gradient iteration vs. number of processors.

Apart from the parallel speedup measurement, we also measured the execution time under condition of constant number of elements per processor. To this end, we initially created a mesh containing 6,192 linear triangular elements. Subsequently, this initial mesh was uniformly subdivided five times yielding a sequence of meshes containing 24,768; 99,072; 396,288; 1,585,152; and 6,340,680 triangular elements. It bears emphasis that each uniform subdivision step raises the number of elements by 4. Thus, when the number of processors is increased accordingly by 4 with each subdivision the number of elements per processor remains, on average, unchanged. We measured the execution time for 3,000 iterations of Jacobi-preconditioned nonlinear conjugate gradient. The execution time per iteration is plotted in figure 5(b). As expected, the execution time is the smallest for the sequential run and increases significantly for parallel runs. We emphasize, however, that the parallel execution times are within 18% of each other, a clear indication of very good parallel performance.

4. Conclusions

Phase-field theory and simulation software have been developed. The theory accounts for deformation twinning in deformable crystalline solids, with equilibrium equations obtained via a variational principle in the null temperature limit. Numerical solutions to weak forms of governing equations are obtained via a conjugate gradient solver and the FE method.

Two fundamental problems in materials physics have been investigated. The first involves homogeneous nucleation of a twin in a Mg single crystal. Critical shear strains for nucleation obtained numerically using the phase-field approach are in reasonable agreement with those obtained analytically in the sharp-interface limit. The second involves twin nucleation in a

$CaCO_3$ single crystal subjected to indentation loading. Long, thin, asymmetric twins with sharp cusp-like tips have been observed in numerical simulations, and are in qualitative agreement with experimental observations.

All results obtained are predictive. The theory and numerical implementation rely only fundamental material properties (e.g., elastic constants and twin boundary surface energies) that can be obtained independently through physical experiments and/or first-principles calculations. Use of the model and software does not require any ad-hoc parameter fitting.

5. References

1. Clayton, J. D.; Knap, J. A Phase Field Model of Deformation Twinning: Nonlinear Theory and Numerical Simulations. Submitted to *Physica D*, 2010.
2. Cahn, J. W.; Hillard, J. E. Free Energy of a Nonuniform System. I. Interfacial Free Energy. *J. Chem. Phys.* **1958**, *28*, 258–267.
3. Allen, S. M.; Cahn, J. W. A Microscopic Theory for Antiphase Boundary Motion and its Application to Antiphase Domain Coarsening. *Acta Metall.* **1979**, *27*, 1085–1095.
4. Steinbach, I.; Pezolla, F.; Nestler, B.; Seebelberg, M.; Prieler, R.; Schmitz, G. J.; Rezende, J.L.L. A Phase Field Concept for Multiphase Systems. *Physica D* **1996**, *94*, 135–147.
5. Steinbach, I.; Apel, M. Multi Phase Field Model for Solid State Transformation with Elastic Strain. *Physica D* **2006**, *217*, 153–160.
6. Fried, E.; Gurtin, M. E. Dynamic Solid-solid Transitions with Phase Characterized by an Order Parameter. *Physica D* **1994**, *72*, 287–308.
7. Gurtin, M. E. Generalized Ginzburg-Landau and Cahn-Hilliard Equations Based on a Microforce Balance. *Physica D* **1996**, *92*, 178–192.
8. Moelins, N.; Blanpain, B.; Wollants, P. An Introduction to Phase-field Modeling of Microstructure Evolution. *Calphad* **2008**, *32*, 268–294.
9. Singer-Loginova, I.; Singer, H. M. The Phase Field Technique for Modeling Multiphase Materials. Rep. *Prog. Phys.* **2008**, *71*, 106501.
10. Levitas, V. A.; Preston, D. L. Three-dimensional Landau Theory for Multivariant Stress-Induced Martensitic Phase Transformations. I. Austenite $\leftrightarrow$ martensite. *Phys. Rev. B* **2002**, *66*, 134206.
11. Clayton, J. D.; Knap, J. Phase Field Modeling of Indentation-induced Twinning in Transparent Crystals, in preparation, 2011.
12. Christian, J. W.; Mahajan, S. Deformation Twinning. *Prog. Mater. Sci.* **1995**, *39*, 1–157.
13. Lee, J. K.; Yoo, M. H. Elastic Strain Energy of Deformation Twinning in Tetragonal Crystals. *Metall. Trans. A* **1990**, *21*, 2521–2530.
14. Slutsky, L. J.; Garland, C. W. Elastic Constants of Magnesium from 4.2K to 300K. *Phys. Rev.* **1957**, *107*, 972–976.

15. Wang, J.; Hirth, J. P.; Tomé, C. N. (1012) Twinning Nucleation Mechanisms in Hexagonal-close-packed Crystals. *Acta Mater.* **2009a**, *57*, 5521–5530.

16. Kronberg, M. L. A Structural Mechanism for the Twinning Process on {1012} in Hexagonal Close Packed Metals. *Acta. Metall.* **1968**, *16*, 29–34.

17. Bell, R. L.; Cahn, R. W. The Dynamics of Twinning and the iInterrelation of Slip and Twinning in Zinc Crystals. *Proc. R. Soc. Lond. A* **1957**, *239*, 494–521.

18. Serra, A.; Pond, R. C.; Bacon, D. J. Computer Simulation of the Structure and Mobility of Twinning Dislocations in h.c.p. Metals. *Acta Metall. Mater.* **1991**, *39*, 1469–1480.

19. Kosevich, A.; Boiko, V. Dislocation Theory of the Elastic Twinning of Crystals. *Sov. Phys. Uspekhi* **1971**, *14*, 286–316.

20. Boiko, V.; Garber, R.; Kosevich, A. *Reversible Crystal Plasticity*; AIP Press: New York, 1994.

21. Lebensohn, R.; Tome, C. A Study of the Stress State Associated with Twin Nucleation and Propagation in Anisotropic Materials. *Philos. Mag. A* **1993**, *67*, 187–206.

22. Dandekar, D.; Ruoff, A. Temperature Dependence of the Elastic Constants of Calcite Between 160° and 300°K. *J. Appl. Phys.* **1968**, *39*, 6004–6009.

23. Bruno, M.; Massaro, F.; Rubbo, M.; Prenicpe, M.; Aquilano, D. (10.4), (01.8), (01.2), and (00.1) Twin Laws of Calcite $CaCO_3$: Equilibrium Geometry of the Twin Boundary Interfaces and Twinning Energy. *J. Cryst. Growth Des.* **2010**, *10*, 3102–3109.

24. Garber, R.; Stepina, E. Rules Governing the Motion of Dislocations During Deformation Twinning. *Sov. Phys. Sol. State* **1965**, *5*, 152–158.

25. XDMF Web site. http://www.xdmf.org (accessed 2010).

26. Gropp, W.; Thakur, R.; Lusk, E. Using MPI-2: *Advanced Features of the Message Passing Interface*; MIT Press: Cambridge, MA, 1999.

27. Toselli, A.; Widlund, O. B. *Domain Decomposition Methods-Algorithms and Theory*, Springer Series in Computational Mathematics, Vol. 34, 2005.

6. Transitions

6.1 Journal Articles

Clayton, J. D.; Knap, J. A Phase Field Model of Deformation Twinning: Nonlinear Theory and Numerical Simulations. Accepted for publication in *Physica D*, 2011.

Clayton, J. D.; Knap, J. Phase Field Modeling of Indentation-induced Twinning in Transparent Crystals. I. Linear Theory, in preparation, 2011.

Clayton, J. D.; Knap, J. Phase Field Modeling of Indentation-induced Twinning in Transparent Crystals. II. Nonlinear Theory, in preparation, 2011.

6.2 Invited Presentations

Clayton**,** J. D.; Knap, J. *Phase Field Modeling of Twin Nucleation in Magnesium and Calcite Single Crystals*, Invited presentation, Center for Advanced Vehicular Systems, Mississippi State University, Starkville, MS, September 28, 2010.

6.3 Transition to ARL Mission Programs

This work will tentatively continue to receive support under the fiscal year 2011 (FY11) WMRD Innovation Project program under the project titled "Twinning in Transparent Materials," which also involves M. Greenfield, J. Swab, and C. Hilton of WMRD. Analytical modeling, phase-field simulations, and physical experiments are planned that will probe twinning phenomena in calcite and alumina single crystals.

List of Symbols, Abbreviations, and Acronyms

Al_2O_3	alumina
AlON	aluminum oxynitride
ARL	U.S. Army Research Laboratory
$CaCO_3$	calcite
CAD	computer-aided design
DoD	Department of Defense
FE	finite element
FY11	fiscal year 2011
HPCMO	High Performance Computing Modernization Office
HPCs	high-performance computers
Mg	magnesium
MPI	Message Passing Interface
V&V	verification and validation
WMRD	Weapons and Materials Research Directorate
XDMF	Extensible Data Model and Format

No of. Copies	Organization
1 (PDF ONLY)	ADMNSTR DEFNS TECHL INFO CTR ATTN DTIC OCP 8725 JOHN J KINGMAN RD STE 0944 FT BELVOIR VA 22060-6218
1 HC	US ARMY RSRCH LAB ATTN RDRL CIM G T LANDFRIED BLDG 4600 ABERDEEN PROVING GROUND MD 21005-5066
3 HCS	US ARMY RSRCH LAB ATTN IMNE ALC HRR MAIL & RECORDS MGMT ATTN RDRL CIM L TECHL LIB ATTN RDRL CIM P TECHL PUB ADELPHI MD 20783-1197
6 HCS	US ARMY RSRCH LAB ATTN RDRL CIH C J KNAP (5 COPIES) ATTN RDRL CIH C P CHUNG BLDG 394 ABERDEEN PROVING GROUND MD 21005-5066
8 HCS	US ARMY RSRCH LAB ATTN RDRL WMP B J CLAYTON (5 COPIES) ATTN RDRL WMP B M GREENFIELD ATTN RDRL WMP B C HOPPEL ATTN RDRL WMP B R BECKER BLDG 390 ABERDEEN PROVING GROUND MD 21005-5066
1 HC	US ARMY RSRCH LAB ATTN RDRL WMM E J SWAB BLDG 4600 ABERDEEN PROVING GROUND MD 21005-5069

TOTAL: 20 (1 ELEC, 19 HCS)

INTENTIONALLY LEFT BLANK.